Hotspot Cooling Performance of Two-Phase Confined Jet Impingement Cooling at the Stagnation Zone

Tanvir Ahmed Chowdhury, and Shawn A. Putnam
Department of Mechanical and Aerospace Engineering
University of Central Florida, Orlando, FL 32816
chowdhurytanvir@knights.ucf.edu, shawn.putnam@ucf.edu

ABSTRACT

Jet impingement can be particularly effective for removing high heat fluxes from local hotspots. Two-phase jet impingement cooling combines the advantages of both the nucleate boiling heat transfer with the single-phase sensible cooling. This study investigates two-phase confined jet impingement cooling of local, laser-generated hotspots in a 100 nm thick Hafnium (Hf) thin film on glass. The jet/nozzle diameter is ∼1.2 mm and the normal distance between the nozzle outlet and the heated surface is ∼3.2 mm. The jet coolants studied are FC 72, Novec 7200, and Ethanol with jet nozzle outlet Reynolds numbers ranging from 250 to 5000. The hotspot area is ∼0.06 mm^2 and the applied hotspot-to-jet heat fluxes range from 20 W/cm^2 to 350 W/cm^2. This heat flux range facilitates studies of both the single-phase and two-phase heat transport mechanisms for heat fluxes up to critical heat flux (CHF). The temporal evolution of the temperature distribution of the laser-heated surface is measured using infrared (IR) thermometry. This study focuses on the stagnation point heat transfer - i.e., the jet potential core is co-aligned with the hotspot center. For ethanol, the CHF is ∼315 W/cm^2 at Re ∼ 1338 with a corresponding heat transfer coefficient of $h \sim 102$ kW/m^2·K. For FC 72, the CHF is ∼94 W/cm^2 at Re ∼ 5000 with a corresponding $h \sim 56$ kW/m^2·K. And for Novec 7200, the CHF is ∼108 W/cm^2 at Re ∼ 4600 with a corresponding $h \sim 50$ kW/m^2·K.

KEY WORDS: Hotspot Cooling, IR Thermography, Confined Jet Impingement

NOMENCLATURE

A	Area, mm^2
D	Diameter of the jet nozzle, mm
Re	Reynolds number
H	Jet nozzle to heated surface distance, mm
HTC, h	Heat transfer coefficient, kW/m^2·K
k	Thermal conductivity, W/m·K
C_p	Volumetric heat capacity, J/K·m^3
P	Laser Power, W
T	Temperature, K
q″	Heat flux, W/cm^2
R	Reflectance

Greek symbols

σ	Absorbance

Subscripts

FS	Fused Silica
HS	Hotspot
f	Fluid
jet	Jet
Hf	Hafnium
th	Thermal
net	Net
eff	Effective

INTRODUCTION

Currently, heat removal from microelectronic devices is a critical challenge that severely impacts the reliability and durability of the devices. Micro-electronic devices are getting smaller, faster, and providing more functions. This trend is leading to more heat flux generation. Additionally, in some cases, the heat flux distribution is not uniform within the device. That leads to extremely high heat flux zones, i.e., hotspots, which are much higher than the average heat flux of the device. Failure to remove the heat flux from these hotspots will lead to significant temperature rise and the eventual failure of the device. According to Mitsutake et al., future devices will require active cooling methods that can remove heat flux of the order of 100 MW/m^2 [1].

For high heat flux removal, liquid cooling is more suitable compared to traditional air cooling. Liquid has higher thermal conductivity and higher heat capacity. As a result, liquid cooling has higher effusivity, resulting in a higher heat transfer coefficient. There has been significant research interest in novel liquid-based convective and phase change cooling methods. Some of these cooling methods include single-phase jet impingement [2], two-phase jet impingement or jet impingement boiling [3], heat pipes [4], thermosyphons [5], immersion cooling [6], micro-channel flow [7], spray cooling [8], pool boiling [9], flow boiling [9], etc.

This work studies the high heat flux cooling method called confined jet impingement cooling. Fig. 1 depicts the flow-field of this confined jet cooling configuration that is applicable for both single-phase and two-phase heat removal in the stagnation zone. This study compares the cooling performance at the stagnation point with multiple coolants (e.g., Ethanol, FC 72, and Novec 7200) and hotspot heat fluxes generated at the stagnation point by a diode laser. In general, this study disseminates the cooling performance in terms of both the

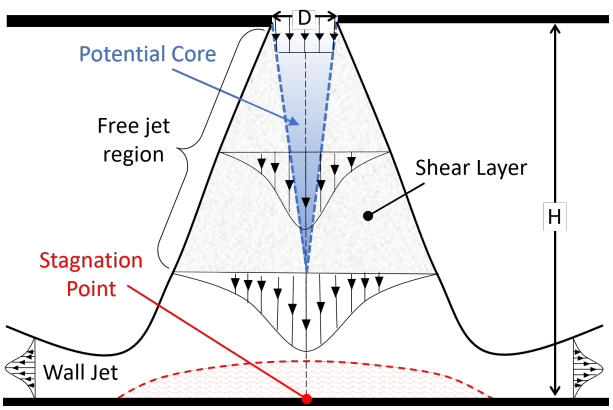

Fig. 1: Confined jet impingement cooling.

hotspot-to-fluid heat flux (q'') and the heat transfer coefficient (h).

The heat transfer coefficient (HTC) is one of the most critical cooling performance metrics for convective cooling methods. HTC is a function of the flow field, cooling device geometry, thermo-fluid properties of the coolant, and the thermal properties of the heated surface. The HTC is defined as heat flux removal per unit temperature rise. Hence, the higher the HTC, the better the cooling method is at maintaining the device temperature within the desired setpoint temperature range during steady or transient heat load conditions.

It is critical to understand the flow field to understand the factors impacting the cooling performance of jet impingement cooling. As illustrated in Fig. 1, after the jet exits the nozzle, a shear layer is formed between the jet and the ambient fluid. Inside this turbulent shear layer is the high-pressure potential core [2]. In the jet flow field, a central part keeps a constant velocity, the same as the velocity at the nozzle outlet. This irrotational part is again the potential core of the jet [10]. Due to the continuous spreading/growth of the shear layer, at a given distance from the jet nozzle, the potential core ceases to exist, and the centerline velocity starts to decrease. This region is called the jet development region. Then, the jet velocity gains a Gaussian profile, and the flow field becomes self-similar. This region is the fully developed jet [2]. The length-scales of the free jet, potential core, and shear layer regions are typically correlated with the ratio between the nozzle height and nozzle diameter (H/D). The shear layer continues to grow as the jet approaches the stagnation zone, generating flow-field instabilities, eddies, and vortex structures. Such vortices are not depicted in Fig.1; however, the vortices interact with surrounding fluid and cause a reduction in the velocity of the jet. This interaction can also effectively increase the flow rate that the heated surface surfaces 'sees' by drawing fluid from the environment. This is defined as the entrainment flow [11], [12].

The potential core typically exists within a distance of 3-4 jet nozzle diameters. After the jet hits the surface, it loses its axial velocity. As a result, the static pressure rises suddenly. The region of the surface, where the jet impinges, is defined as the stagnation zone. Surrounding the stagnation zone region is the acceleration region - i.e., the flow-field region where the flow direction begins to transition from normal to the surface to parallel to the surface. Lastly, the radial region is where the fluid velocity is parallel to the surface. This region is also called the wall jet region. The velocity profile in this region is comparable to the flat plate boundary-layer profile, but this region has two distinct shear layers — one with the plate and the other with the ambient fluid at the top. Moreover, due to these two shear layers, turbulence in a wall jet is much higher than that of the boundary layer flow. Like the free jet region, the wall jet region also gains a self-similar profile at large radial distances from the stagnation zone [12].

Over the last several decades, research on predicting the HTC for various experimental conditions has been of utmost importance [1], [2], [13]–[29], [29]–[32]. One of the key parameters for submerged/confined jet impingement is the separation distance between the jet nozzle outlet and the heated wall surface H (or the ratio of H/D). The HTC decreases when the $H/D < 2$ as the jet does not have enough space to become fully developed. It has been found that maximum HTCs are achieved when $H/D \leq 5$, when the $H/D > 6$, the HTC decreases significantly [2]. Another critical parameter for confined jet impingement is the mean jet velocity (or jet Reynolds number, Re). An increase in jet impingement velocity (or jet Reynolds number) results in an increase in the HTC. The HTC is found to be the highest within the stagnation zone. The peak or maximum HTC is either at the stagnation point or the edge of the stagnation zone. Webb et al. [33], and Zuckerman et al. [2] have compiled local HTC profiles in the radial direction. Generally, the HTC gradually decreases as the radial distance from the stagnation increases.

One of the most effective ways to gain greater cooling performance is through introducing phase change (liquid-to-vapor) in jet flow. The point at a jet impingement boiling curve, where the jet flow transitions from single phase to two-phase is defined as the onset of nucleate boiling. The nucleate boiling regime is defined by the two-phase heat transfer process where small vapor bubbles are created that quickly detach themselves from the heated surface; thus, enhancing the overall rate of heat transfer. The upper limit of this regime is the Critical Heat Flux (CHF). Beyond this point, heat transfer performance drops, and the boiling curve falls into the transition boiling regime. In this regime, unstable vapor blankets form and collapse, accompanied by intermittent wetting of the surface. Hence, it is crucial to know the onset boiling heat flux and the CHF to keep the boiling curve in the nucleate boiling regime and achieve the highest heat transfer performance.

CHF occurs due to the slower liquid supply rate to the heated surface compared to the vapor production rate. Katto and Kunihiro [34] were among the first to suggest that the impinging liquid jet can increase the fluid supply to the heater and increase the CHF. Most studies indicate that with increasing jet velocity, the CHF will increase [34]–[36]. Faster jet velocity helps pierce the vapor layer and provides continuous liquid supply to the heated surface. This results in the widening

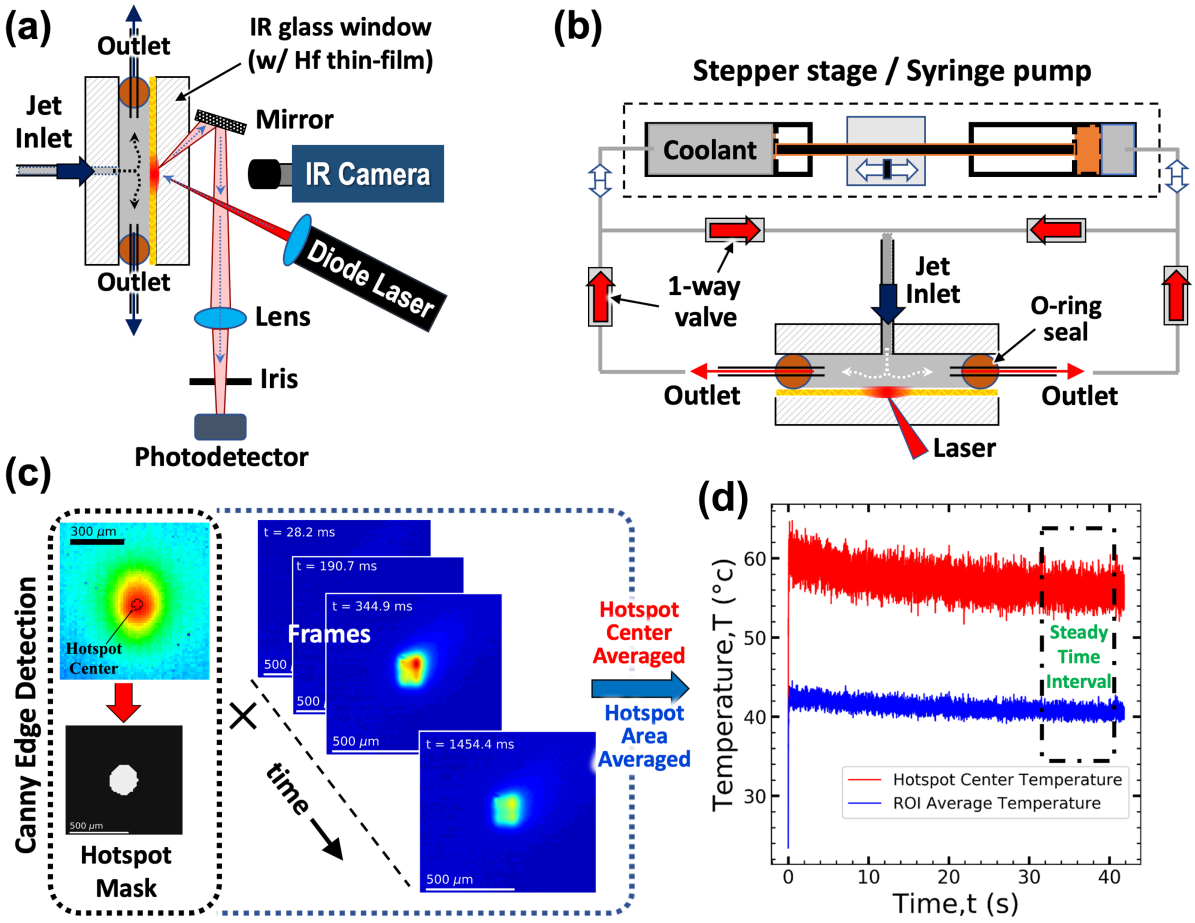

Fig. 2: Overview of the two-phase confined jet impingement setup for cooling local hotspots generated by a focused diode laser. (a) Laser heating schematic emphasizing the in-situ IR thermometry method and laser power monitoring with a photodetector. (b) Schematic of the jet impingement flow-loop using a dual syringe pump configuration and four one-way flow valves. (c) Schematic illustration of hotspot segmentation from the IR image of hotspot, and the tracking of the hotspot center temperature and area-averaged temperature. (d) Temporal evolution of the averaged hotspot temperature after the initiation of laser diode heating at $t = 0$ seconds.

of the nucleate boiling regime. However, according to some studies [35], [37], this CHF increment is only significant at lower velocities, while at higher jet velocities, the increment in CHF is not prominent. Another critical parameter that impacts the CHF greatly is jet subcooling. Subcooling is defined as the difference between the jet temperature at the nozzle outlet and the coolant boiling point. Subcooling typically increases the CHF [38]–[40]. Due to subcooling, the vapor bubbles are absorbed in bulk fluid via sensible heat transfer to the bulk fluid. As a result, subcooling helps reduce the void fraction and increases the rate of sensible heat transfer [3].

While all of the aforementioned parameters affecting the CHF have been extensively studied, almost all these studies focus on either the constant surface temperature or constant heat flux configurations with the heated surface region being much greater than the width of the stagnation zone. This study focuses on the highly localized, micro-scale hotspot heat removal process by two-phase jet impingement cooling at the stagnation point, where the jet and the hotspot are co-aligned and hotspot size (D_{HS}) is small in comparison to the jet nozzle diameter (or width of the stagnation zone) - i.e., $D_{HS}/D \approx 0.23$. Dielectric liquids Novec 7200 (made by 3M Inc.), FC 72, and Ethanol were chosen as the jet coolants. The boiling onset and the CHF are studied as a function of inlet jet velocity (or jet Reynolds number). The jet Reynolds number from the nozzle outlet is varied from Re$\approx$ 250 to Re$\approx$ 5000. Heat transfer data is also provided with these different fluids for the confined, stagnant fluid condition (i.e., Re$\approx$ 0). The heat transfer performance data for these different coolants are disseminated using traditional cooling performance curves, facilitating subsequent use of the CHF, incipient, nucleate boiling results by the heat transfer community in other two-phase, hotspot cooling architectures.

EXPERIMENTAL SETUP

This confined jet impingement cooling study uses a simple confined jet chamber based on an O-ring seal between two

fused silica (FS) glass windows. One of the glass windows is coated with a thin film Hafnium (Hf). This Hf thin film coating acts as both the heater and thermometer of the experimental setup. The Hf-glass window was fabricated by depositing $\sim$100 nm of Hf on an Infrared (IR) transparent FS glass window via DC magnetron sputtering. A diode laser locally heats the Hf thin-film and creates the hotspot heat source, as depicted in Fig. 2a. The jet coolant is issued through the center of the glass window by a syringe needle, such that the jet creates a normal angle of incidence while impinging on the Hf thin-film. Additionally, two syringe needles, passing through the O-ring seal, function as the outlets for the spent flow. For this study, H/D is kept constant at a value of ≈ 2.64, where the nozzle outlet to heated surface distance is $H \approx 3.175$ mm and $D \approx 1.2$ mm. The later sections describe the hotspot heating in detail.

Fig. 2a presents the hotspot generation by heating with a focused diode laser, the cooling of the hotspot by the impinging confined jet, and the subsequent spatiotemporal temperature measurement of the Hf thin film using the IR camera schematically. A blue laser (450 nm), partially absorbed by the Hf thin film ($R \sim 45$ %, transmission < 0.1 %), creates the hotspot. The hotspot size in the Hf thin film is maintained to be $\sim$ 0.06 mm^2 (0.138 mm in radius) with the help of a focusing lens. A LED current-voltage driver is used to control the laser power. The reflected laser light from the Hf thin film is captured by a photo-detector, where the output voltage of the photo-detector is monitored by an oscilloscope, as represented in Fig. 2a. The response of the photo-detector allows in-situ temporal heat input monitoring.

A jet flow-loop configuration with a dual syringe pump cools the hotspot, as depicted in Fig. 2b. A computer-controlled stepper stage is connected with two stainless steel piston syringes. When the stepper stage moves in one direction, the coolant is simultaneously displaced out of one piston syringe and into the other piston syringe. The combination of four one-way valves provides a continuous jet flow regardless of the piston pumping direction. The later section describes the spatiotemporal temperature evolution monitoring in more detail.

A FLIR IR camera (spectral sensitivity: 1.5 - 5 μm, pixel size $\sim$ 14.42 μm, window size: 160 $\times$ 128, and frame rate: 603 frames per second) is used to capture the spatiotemporal temperature of the hotspot. A K-type thermocouple is used to calibrate the IR camera. The accuracy of the IR camera temperature is within $\pm$ 0.2 $-$ 0.6 K when the temperature is below 40 $^\circ C$, whereas the uncertainty increases to $\pm$ 1 $-$ 2 K when the temperature is above 45 $^\circ C$. The emissivity of the Hf thin film and the transmissivity of the IR transparent FS window were measured by following the procedure outlined by FLIR [41].

As the heating condition is for a local, micro-scale hotspot, the captured IR frames need post-processing to extract the hotspot temperature. Fig. 2c presents how the IR images are processed to extract the spatiotemporal temperature evolution. The hotspot depicted in the upper left in Fig. 2c corresponds to laser diode heating of a stagnant coolant pool inside the chamber (i.e., no impinging jet (Re$\approx$ 0) and a low laser power to avoid incipient or nucleate boiling over the hotspot). The subsequent series of hotspot images corresponds to laser diode heating at near critical heat fluxes with an impinging jet (Re$\approx$ 5000). The Hf thin-film is assumed to have a thickness-independent hotspot temperature since the Hf thin-film is only $\sim$100 nm in thickness. However, the in-plane temperature distribution in Hf thin-film is highly nonuniform (as depicted in Fig. 2c). At low laser powers (or wall heat fluxes) the temperature profile follows a gaussian distribution, whereas at higher laser powers (or wall heat fluxes) the temperature profile follows a top-hat distribution with some quadrant-heating characteristics due to the quadrant-design of the laser diode source.

For spatiotemporal analysis of hotspot temperature (Fig.2c), we use both the Canny edge detection method [42] and the floodfill method to segment the hotspot region-of-interest (ROI). A binary mask is multiplied with acquired IR camera images; thus, extracting the temporal temperature information within the hotspot. Then, the area average of the hotspot temperature for each frame is calculated, which provides the temporal trends of the area-averaged (or ROI-averaged) hotspot temperature. For example, Fig. 2d shows the temporal plot of the hotspot area-averaged temperature and hotspot center temperature based on an applied hotspot-to-jet heat flux of 91.2 W/cm^2, at $Re = 5000$ for Novec 7100 coolant [43]. Fig. 2d also shows how the temperature initially overshoots after the laser heating is initiated (i.e., the dramatic hotspot temperature excursion after the heat flux is applied at $t =$ 0 seconds). Then, the average hotspot temperature gradually decreases (with rapid millisecond temperature fluctuations) before becoming 'steady'. The boxed region in Fig. 2d depicts the time interval where the temporal temperature approximates a steady-state profile. All the temperature data presented in this study corresponds to this steady-state time interval regime. Also, the inlet jet coolant temperatures for all the confined jet impingement experiments were $T_{jet} \sim 22 - 23\ ^\circ C$.

RESULTS & DISCUSSION

Accurate measurement of the wall heat flux removed by the coolant and the heat transfer coefficient requires an understanding of the conjugate heat transfer in the Hf-coated glass substrate. While the Hf film is $\sim$100 nm thick, there is substantial in-plane thermal conduction. The area-averaged hotspot heat flux in the Hf thin-film heater $q''_{\rm net}$ can be defined as:

$$q''_{\rm net} = \frac{P\sigma}{A_{\rm HS}}, \tag{1}$$

where P is the laser power output, $\sigma = 1 - R$ is the amount of absorbed laser light, R is the reflectance of the Hf thin film, and $A_{\rm HS}$ is the hotspot area. Since the applied heat flux on the Hf thin film is removed by the fluid, Hf thin-film, and the FS glass substrate, the relation among the applied heat flux,

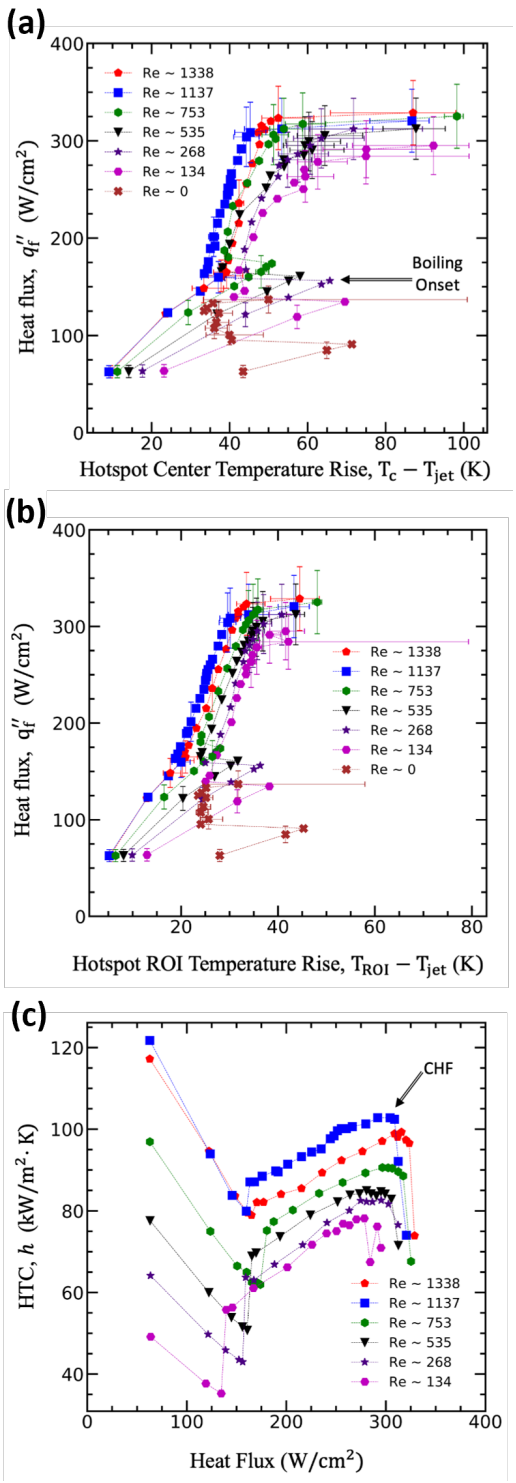

Fig. 3: Single and two-phase jet impingement cooling data for Ethanol with jet nozzle Reynolds numbers ranging from Re∼0 (i.e., a stagnant, confined pool) to Re∼1338. (a) Wall heat flux verses the temperature rise at the hotspot center. (b) Wall heat flux verses the ROI-averaged, hotspot temperature rise. (c) Hotspot area-averaged HTC verses the wall heat flux (134$\lesssim$ Re $\lesssim$1338).

the heat flux removed by the fluid, and the heat flux removed by the glass substrate can be expressed as:

$$q''_{\text{net}} = q''_{\text{f}} + q''_{\text{FS}}, \tag{2}$$

where q''_{FS} is the heat flux removed by the glass window and q''_{f} is the heat flux removed by the coolant. q''_{f} can be calculated using the following equation:

$$q''_{\text{f}} = q''_{\text{net}} \left(\frac{e^{\text{eff}}_{\text{th,f}}}{e^{\text{eff}}_{\text{th,f}} + e^{\text{eff}}_{\text{th,FS}}} \right), \tag{3}$$

where $e_{\text{th,f}}$ and $e_{\text{th,FS}}$ are the effective thermal effusivities of the fluid and the glass substrate, respectively. The thermal effusivities are defined as:

$$\begin{aligned} e_{\text{th,f}} &= \sqrt{k^{\text{eff}}_{\text{f}} C_{\text{p,f}}} \\ e_{\text{th,FS}} &= \sqrt{k^{\text{eff}}_{\text{FS}} C_{\text{p,FS}}}, \end{aligned} \tag{4}$$

where $C_{\text{p,f}}$ and $C_{\text{p,FS}}$ are the volumetric heat capacities of the fluid/coolant, and the glass substrate, respectively, and $k^{\text{eff}}_{\text{f}}$ and $k^{\text{eff}}_{\text{FS}}$ are the effective thermal conductivities of the fluid and the glass substrate, respectively. The transient heat transfer from the laser-induced disc source of heat in the Hf thin-film of constant heat flux (q''_{f}) is anisotropic [44]. Therefore, the effective thermal conductivities of the fluid and glass substrates can account for the in-plane conduction in the Hf thin-film via

$$\begin{aligned} k^{\text{eff}}_{\text{f}} &= k^{1/3}_{\text{f}} k^{2/3}_{\text{Hf}} \\ k^{\text{eff}}_{\text{FS}} &= k^{1/3}_{\text{FS}} k^{2/3}_{\text{Hf}}, \end{aligned} \tag{5}$$

where k_{f}, k_{FS}, and k_{Hf} are the thermal conductivities of the fluid coolant, the glass substrate, and the Hf thin-film, respectively [43]. These expressions for the effective thermal conductivities predict the spatiotemporal hotspot temperatures for both jets and stagnant fluids (e.g., air, Ethanol.) with both modulated (periodic) and steady heating by the laser very accurately. Detailed discussion about these expressions can be found in previous publication by the authors [43].

The area-averaged heat transfer coefficient (h) can be expressed as:

$$h = \frac{q''_{\text{f}}}{\Delta T}, \tag{6}$$

where ΔT is the difference between the coolant temperature (T_{jet}) and the time-averaged hotspot area-averaged temperature (T_{ROI}). As stated previously, this study presents the cooling performance of the two-phase confined jet impingement by evaluating the steady period.

Fig. 3 provides experimental data for single and two-phase confined jet impingement cooling with ethanol for a wide range of different jet nozzle Reynolds numbers. The heat transfer data is plotted in terms of the wall-to-jet heat flux, the hotspot center temperature rise, the area-averaged hotspot temperature rise, and the area-averaged, hotspot heat transfer coefficient. Fig. 3a and Fig. 3b present the hotspot center temperature rise and the ROI averaged temperature rise at the steady time interval. In Figs. 3a and 3b, experimental error bars are only provided at selected Reynolds number values that

correspond to (i) five data points with the highest uncertainties and (ii) two data points with the lowest uncertainties. The uncertainty in laser power output measurements, the reflectivity of the Hf surface, hotspot area, inlet jet temperature, and the fluctuations in heated surface temperature were all considered while calculating 95% confidence intervals. The flow-field is initially single-phase at the lower wall heat fluxes, where the fluctuations in hotspot wall temperature are the result of the motion of the eddies present in the jet flow-field. At higher heat fluxes, when the flow is in the two-phase regime, the boiling events further increase fluctuations in the hotspot temperature.

At high heat fluxes, the hotspot center temperature fluctuations are of the order of 40-60 $^{\circ}C$, and the ROI average temperature fluctuation is of the order of 30-40 $^{\circ}C$. These high fluctuations in temperature occur due to the dry-out and subsequent wetting of the hotspot region at heat fluxes over a critical heat flux. Hence, to avoid these extreme temperature rise/fluctuations and potential device failure from the high-temperature rise and thermal fatigue, the CHF needs to be mapped in terms of the jet Reynolds number. Fig. 3a and 3b show that the same temperature can be maintained at a lower Reynolds number by introducing nucleate boiling in jet cooling. Therefore, this study also maps the onset of nucleate boiling in terms of the jet Reynolds number.

In order to extract the limits of the nucleate boiling regime and compare among the experiments systematically, this study defines those limits or the transitional heat fluxes. In some cases, when the hotspot center temperature approaches the boiling point of the coolant, the HTC ($q''/\Delta T$) increases or $\frac{\partial^2 q''}{\partial T^2}$ becomes positive. This point is defined as the transitional heat flux for the onset of nucleate boiling. On the other hand, in some cases, the temperature rises above the boiling point before overshooting to a lower temperature, and the boiling initiates. The point at which the hotspot temperature overshoots to a lower temperature is defined as transitional heat flux for incipient boiling. According to Zhou et al., the liquid wetting angle is greater than the effective cone angle of the nucleation cavities, and the liquid can not fill those cavities. Boiling occurs once the vapor embryos obtain sufficient energy to nucleate and separate from the nucleation cavities [15]. On the other hand, as illustrated in Fig. 3c, CHF is defined as the point where the nucleate boiling HTC reaches a local maximum (or when $\partial h/\partial q'' < 0$).

Fig. 4 overviews the extracted stagnation point transitional heat flux data for (a) Novec 7200, (b) Ethanol, and (c) FC 72 coolants as a function of jet Reynolds number. The boiling onset and the CHF are defined as the transitional heat fluxes. Overall, for all of the coolants, greater jet velocity/Reynolds number extends the nucleate boiling regime. The CHF and boiling onset increase rapidly with the increasing jet velocity when the flow is laminar. For Ethanol, the CHF increases from ~132 W/cm^2 to ~290 W/cm^2 for a small increment in Reynolds number from 0 to ~268. When the flow approaches the transitional/turbulent flow regime, the rate of the transitional heat flux increment decreases. Nonetheless, the CHF and the boiling onset increase with the greater Reynolds number, and the nucleate boiling regime becomes wider. Previous a publication by the authors presented that for Novec

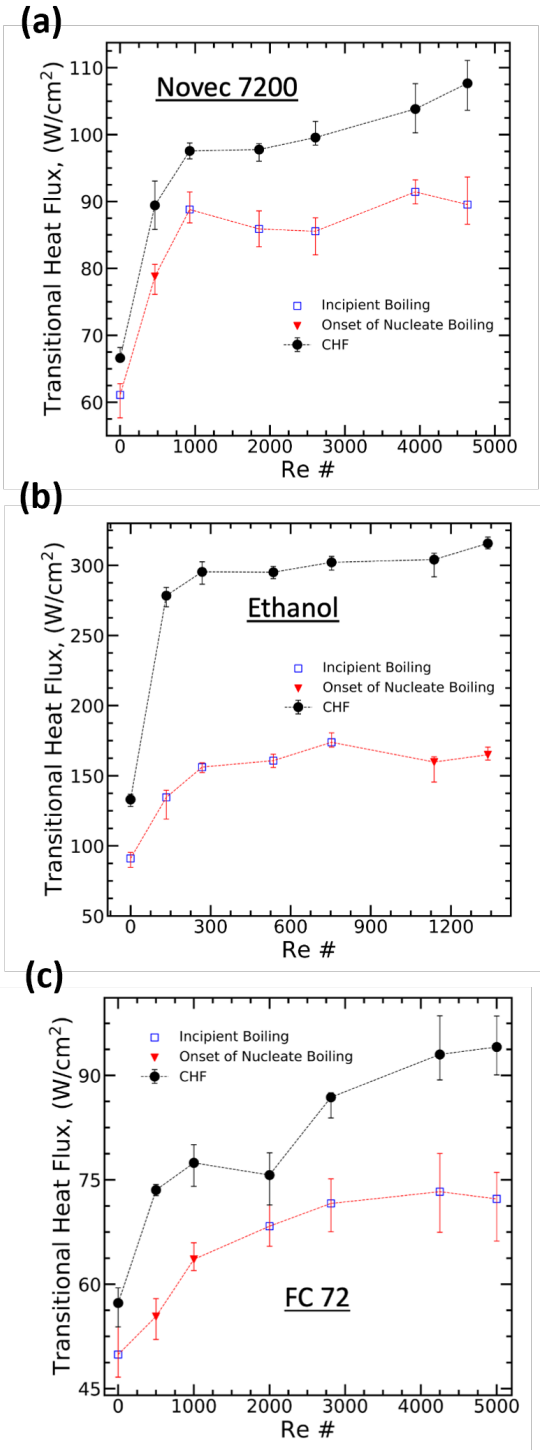

Fig. 4: Transitional heat flux data at the stagnation point for two-phase, confined jet impingement cooling using (a) Novec 7200, (b) Ethanol, and (c) FC 72 coolants. The heat transfer data are based on both the hotspot area-averaged wall-to-coolant heat flux and the area-averaged hotspot temperature rise ($0 \lesssim$ Re $\lesssim 5000$).

7100, the incipient boiling occurs at lower Reynolds number (laminar regime) and the onset of nucleate boiling occurs at higher Reynolds number (transitional/turbulent regime) [43]. However, the current study with the three different coolants has shown that this trend is not valid for all the coolants. Further investigations with different coolants and hotspot sizes are needed to gain a theoretical understanding of this seemingly irregular pattern of the incipient boiling occurrence.

CONCLUSION

This study investigated the stagnation point cooling performance for confined two-phase jet impingement cooling of local hotspots as a function of both the wall-to-jet heat flux and the jet Reynolds number. FC 72, Novec 7200, and Ethanol were used as coolants. The key transitional heat fluxes measured in this work include the incipient boiling, nucleate boiling, and critical heat flux. All these transitional heat fluxes were observed to increase in magnitude with corresponding increases the jet velocity (or jet Reynolds number), where the heat flux regime for the onset nucleate boiling also broadened in width with the increasing jet velocity. In the laminar flow regime, for Novec 7200 and Ethanol, a small increment jet Reynolds number (ΔRe$\leq$ 1000) resulted in nearly a $\sim$100$\%$ enhancement in CHF (i.e., a CHF enhancement relative to the stagnant/confined pool CHF for Re$\approx$ 0). This key result supports that hotspot cooling with two-phase jet impingement can dramatically enhance the nucleate boiling heat transfer regime with relatively small jet impingement velocities; thus, enabling high heat flux removal from hotspots with Re$<$ 500. Moreover, with impinging ethanol jets, a CHF of $\sim$315 W/cm^2 was recorded at Re $\sim$ 1338 with a corresponding maximum heat transfer coefficient of $h \approx$ 102 kW/m^2·K. Finally, while the observed onsets for incipient and nucleate boiling were shown to be directly proportional to the inlet jet velocity, the relation between the jet velocity and the incipient boiling occurrence remains difficult to predict. Further investigations with larger hotspots are also needed (e.g., 0.2$\leq D_{HS}/D \leq$ 3) to confirm that similar cooling performances can be achieved with larger hotspots (or greater overall heat loads at comparable hotspot heat fluxes).

Acknowledgments

This material is based on research partially sponsored by the U.S. Israel Binational Science Foundation (Grant No. 2016399) and research partially sponsored by the National Science Foundation (Grant No. 1653396). The views and conclusions contained herein are those of the authors and should not be interpreted as necessarily representing the official policies or endorsements, either expressed or implied, of the U.S. Government, departments thereof, or the Office of the US Israel Binational Science Foundation. The authors thank the incredibly helpful feedback from Gennady Ziskind and Tomer Shockner. The authors also thank Khan Mohammad Rabbi and Chance Brewer. The authors are grateful for NumPy [45], SciPy [46], Pandas [47], Matplotlib [48] packages that helped immensely during the data analysis.

References

[1] Y. Mitsutake and M. Monde, "Ultra High Critical Heat Flux During Forced Flow Boiling Heat Transfer With an Impinging Jet ," *Journal of Heat Transfer*, vol. 125, no. 6, pp. 1038–1045, 11 2003. [Online]. Available: https://doi.org/10.1115/1.1621899

[2] N. Zuckerman and N. Lior, "Impingement Heat Transfer: Correlations and Numerical Modeling," *Journal of Heat Transfer*, vol. 127, no. 5, pp. 544–552, 05 2005. [Online]. Available: https://doi.org/10.1115/1.1861921

[3] V. Devahdhanush and I. Mudawar, "Review of critical heat flux (chf) in jet impingement boiling," *International Journal of Heat and Mass Transfer*, vol. 169, p. 120893, 2021. [Online]. Available: https://www.sciencedirect.com/science/article/pii/S0017931020338254

[4] H. Jouhara, A. Chauhan, T. Nannou, S. Almahmoud, B. Delpech, and L. Wrobel, "Heat pipe based systems - advances and applications," *Energy*, vol. 128, pp. 729–754, 2017. [Online]. Available: https://www.sciencedirect.com/science/article/pii/S0360544217305935

[5] S. Noie, "Heat transfer characteristics of a two-phase closed thermosyphon," *Applied Thermal Engineering*, vol. 25, no. 4, pp. 495–506, 2005. [Online]. Available: https://www.sciencedirect.com/science/article/pii/S1359431104001838

[6] P. Birbarah, T. Gebrael, T. Foulkes, A. Stillwell, A. Moore, R. Pilawa-Podgurski, and N. Miljkovic, "Water immersion cooling of high power density electronics," *International Journal of Heat and Mass Transfer*, vol. 147, p. 118918, 2020. [Online]. Available: https://www.sciencedirect.com/science/article/pii/S0017931019336002

[7] B. Agostini, J. R. Thome, M. Fabbri, and B. Michel, "High heat flux two-phase cooling in silicon multimicrochannels," *IEEE Transactions on Components and Packaging Technologies*, vol. 31, no. 3, pp. 691–701, 2008.

[8] G. Liang and I. Mudawar, "Review of spray cooling – part 2: High temperature boiling regimes and quenching applications," *International Journal of Heat and Mass Transfer*, vol. 115, pp. 1206–1222, 2017. [Online]. Available: https://www.sciencedirect.com/science/article/pii/S0017931017302958

[9] M. Shojaeian and A. Koşar, "Pool boiling and flow boiling on micro- and nanostructured surfaces," *Experimental Thermal and Fluid Science*, vol. 63, pp. 45–73, 2015. [Online]. Available: https://www.sciencedirect.com/science/article/pii/S0894177714003215

[10] K. Choo, B. K. Friedrich, A. W. Glaspell, and K. A. Schilling, "The influence of nozzle-to-plate spacing on heat transfer and fluid flow of submerged jet impingement," *International Journal of Heat and*

Mass Transfer, vol. 97, pp. 66–69, 2016. [Online]. Available: https://www.sciencedirect.com/science/article/pii/S0017931015308218

[11] S. A. Striegl and T. E. Diller, "An Analysis of the Effect of Entrainment Temperature on Jet Impingement Heat Transfer," *Journal of Heat Transfer*, vol. 106, no. 4, pp. 804–810, 11 1984. [Online]. Available: https://doi.org/10.1115/1.3246755

[12] Z. Xu, H. Hangan, and P. Yu, "Analytical Solutions for a Family of Gaussian Impinging Jets," *Journal of Applied Mechanics*, vol. 75, no. 2, 02 2008, 021019. [Online]. Available: https://doi.org/10.1115/1.2775502

[13] S. Ndao, Y. Peles, and M. K. Jensen, "Experimental investigation of flow boiling heat transfer of jet impingement on smooth and micro structured surfaces," *International Journal of Heat and Mass Transfer*, vol. 55, no. 19, pp. 5093 – 5101, 2012. [Online]. Available: http://www.sciencedirect.com/science/article/pii/S0017931012003225

[14] C.-F. Ma and A. Bergles, "Jet impingement nucleate boiling," *International Journal of Heat and Mass Transfer*, vol. 29, no. 8, pp. 1095 – 1101, 1986. [Online]. Available: http://www.sciencedirect.com/science/article/pii/0017931086901407

[15] D. Zhou, C. Ma, and J. Yu, "Boiling hysteresis of impinging circular submerged jets with highly wetting liquids," *International Journal of Heat and Fluid Flow*, vol. 25, no. 1, pp. 81–90, 2004. [Online]. Available: https://www.sciencedirect.com/science/article/pii/S0142727X03001280

[16] S. N. Joshi and E. M. Dede, "Effect of sub-cooling on performance of a multi-jet two phase cooler with multi-scale porous surfaces," *International Journal of Thermal Sciences*, vol. 87, pp. 110 – 120, 2015. [Online]. Available: http://www.sciencedirect.com/science/article/pii/S1290072914002403

[17] M. J. Rau, E. M. Dede, and S. V. Garimella, "Local single- and two-phase heat transfer from an impinging cross-shaped jet," *International Journal of Heat and Mass Transfer*, vol. 79, pp. 432 – 436, 2014. [Online]. Available: http://www.sciencedirect.com/science/article/pii/S0017931014006991

[18] L. Qiu, S. Dubey, F. H. Choo, and F. Duan, "Recent developments of jet impingement nucleate boiling," *International Journal of Heat and Mass Transfer*, vol. 89, pp. 42–58, 2015. [Online]. Available: https://www.sciencedirect.com/science/article/pii/S0017931015005086

[19] P. Valiorgue, T. Persoons, A. McGuinn, and D. Murray, "Heat transfer mechanisms in an impinging synthetic jet for a small jet-to-surface spacing," *Experimental Thermal and Fluid Science*, vol. 33, no. 4, pp. 597 – 603, 2009. [Online]. Available: http://www.sciencedirect.com/science/article/pii/S0894177708001763

[20] D. B. M. M. F. Colin Glynn, Tadhg O'Donovan, "Jet impingement cooling," *Proceedings of the 9th UK National Heat Transfer Conference*, pp. 5–6, 2005.

[21] Y. hao Qiu and Z. hua Liu, "Critical heat flux of steady boiling for saturated liquids jet impinging on the stagnation zone," *International Journal of Heat and Mass Transfer*, vol. 48, no. 21, pp. 4590 – 4597, 2005. [Online]. Available: http://www.sciencedirect.com/science/article/pii/S0017931005004023

[22] S.-M. Lin, H.-F. Liu, W.-R. Wang, S. Y. Lee, C.-Y. Cheng, and C.-Y. Li, "Optimum design and heat transfer correlation equation of a mini radiator with jet impingement cooling," *Applied Thermal Engineering*, vol. 89, pp. 727 – 737, 2015. [Online]. Available: http://www.sciencedirect.com/science/article/pii/S1359431115006249

[23] C.-B. Kim, C. Leng, X.-D. Wang, T.-H. Wang, and W.-M. Yan, "Effects of slot-jet length on the cooling performance of hybrid microchannel/slot-jet module," *International Journal of Heat and Mass Transfer*, vol. 89, pp. 838 – 845, 2015. [Online]. Available: http://www.sciencedirect.com/science/article/pii/S0017931015006122

[24] Z. Zhao, Y. Peles, and M. K. Jensen, "Microjet impingement boiling on a structured-porous surface," *ASME 2012 Third International Conference on Micro/Nanoscale Heat and Mass Transfer*, pp. 411–417, 2013.

[25] X. Liu, L. A. Gabour, and V. Lienhard, J. H., "Stagnation-Point Heat Transfer During Impingement of Laminar Liquid Jets: Analysis Including Surface Tension," *Journal of Heat Transfer*, vol. 115, no. 1, pp. 99–105, 02 1993. [Online]. Available: https://doi.org/10.1115/1.2910677

[26] Y.-J. Chen, Y.-Y. Li, and Z.-H. Liu, "Experimental study on the stagnation line heat transfer characteristics with high-velocity free slot jet impingement boiling," *International Journal of Heat and Mass Transfer*, vol. 91, pp. 282 – 292, 2015. [Online]. Available: http://www.sciencedirect.com/science/article/pii/S0017931015008327

[27] T. Park, H. Choi, J. Yoo, and S. Kim, "Streamline upwind numerical simulation of two-dimensional confined impinging slot jets," *International Journal of Heat and Mass Transfer*, vol. 46, no. 2, pp. 251 – 262, 2003.

[28] J. W. Baughn, A. E. Hechanova, and X. Yan, "An Experimental Study of Entrainment Effects on the Heat Transfer From a Flat Surface to a Heated Circular Impinging Jet," *Journal of Heat Transfer*, vol. 113, no. 4, pp. 1023–1025, 11 1991. [Online]. Available: https://doi.org/10.1115/1.2911197

[29] T. Germain, T. A. Chowdhury, J. Carter, and S. A. Putnam, "Measuring heat transfer coefficients for microchannel jet impingement using time-domain thermoreflectance," in *2018 17th IEEE Intersociety Conference on Thermal and Thermomechanical Phenomena in Electronic Systems (ITherm)*, May 2018, pp. 449–454.

[30] K. M. Rabbi, J. Carter, and S. A. Putnam, "Understanding

pulsed jet impingement cooling by instantaneous heat flux matching at solid-liquid interfaces," *Phys. Rev. Fluids*, vol. 5, p. 094003, Sep 2020. [Online]. Available: https://link.aps.org/doi/10.1103/PhysRevFluids.5.094003

[31] E. Wang, L. Zhang, L. Jiang, J.-M. Koo, J. G. Maveety, E. Sanchez, K. Goodson, and T. W. Kenny, "Micromachined jets for liquid impingement cooling of vlsi chips," *Journal of Microelectromechanical Systems*, vol. 13, pp. 833–842, 2004.

[32] T. A. Chowdhury, C. Brewer, and S. A. Putnam, "Hotspot cooling performance of a submerged water jet via infrared thermometry," in *2020 19th IEEE Intersociety Conference on Thermal and Thermomechanical Phenomena in Electronic Systems (ITherm)*, 2020, pp. 166–172.

[33] B. Webb and C.-F. Ma, "Single-phase liquid jet impingement heat transfer," ser. Advances in Heat Transfer, J. P. Hartnett and T. F. Irvine, Eds. Elsevier, 1995, vol. 26, pp. 105 – 217. [Online]. Available: http://www.sciencedirect.com/science/article/pii/S006527170870296X

[34] Y. Katto and M. Kunihiro, "Study of the mechanism of burn-out in boiling system of high burn-out heat flux," *Bulletin of JSME*, vol. 16, no. 99, pp. 1357–1366, 1973.

[35] V. Devahdhanush and I. Mudawar, "Critical heat flux of confined round single jet and jet array impingement boiling," *International Journal of Heat and Mass Transfer*, vol. 169, p. 120857, 2021. [Online]. Available: https://www.sciencedirect.com/science/article/pii/S0017931020337893

[36] Y. Katto and M. Monde, "Mechanism of burn-out in a high heat-flux boiling system with an impinging jet," *Transactions of the Japan Society of Mechanical Engineers*, vol. 41, no. 341, pp. 306–314, 1975.

[37] Y. Katto and M. Shimizu, "Upper Limit of CHF in the Saturated Forced Convection Boiling on a Heated Disk with a Small Impinging Jet," *Journal of Heat Transfer*, vol. 101, no. 2, pp. 265–269, 05 1979. [Online]. Available: https://doi.org/10.1115/1.3450958

[38] I. Mudawar and D. Wadsworth, "Critical heat flux from a simulated chip to a confined rectangular impinging jet of dielectric liquid," *International Journal of Heat and Mass Transfer*, vol. 34, no. 6, pp. 1465–1479, 1991. [Online]. Available: https://www.sciencedirect.com/science/article/pii/001793109190289Q

[39] K. A. Estes and I. Mudawar, "Comparison of Two-Phase Electronic Cooling Using Free Jets and Sprays," *Journal of Electronic Packaging*, vol. 117, no. 4, pp. 323–332, 12 1995. [Online]. Available: https://doi.org/10.1115/1.2792112

[40] M. E. Johns and I. Mudawar, "An Ultra-High Power Two-Phase Jet-Impingement Avionic Clamshell Module," *Journal of Electronic Packaging*, vol. 118, no. 4, pp. 264–270, 12 1996. [Online]. Available: https://doi.org/10.1115/1.2792162

[41] R. Danjoux, "Window and external optics transmittance," http://support.flir.com, 'A817-T560472_A-en-US Technical publication 60 Window or External Optics Transmittance.pdf', accessed: 2020-03-04.

[42] J. Canny, "A computational approach to edge detection," *IEEE Transactions on Pattern Analysis and Machine Intelligence*, vol. PAMI-8, no. 6, pp. 679–698, Nov 1986.

[43] *Hotspot Cooling Performance for Submerged Confined Two-Phase Jet Impingement Cooling*, ser. International Electronic Packaging Technical Conference and Exhibition, vol. ASME 2021 International Technical Conference and Exhibition on Packaging and Integration of Electronic and Photonic Microsystems, 10 2021, v001T08A003. [Online]. Available: https://doi.org/10.1115/IPACK2021-69317

[44] H. S. Carslaw and J. C. Jaeger, *Conduction of Heat in Solids*, 2nd ed. New York: Oxford University Press, 1959, pp. 257,260,264.

[45] T. Oliphant, "NumPy: A guide to NumPy," USA: Trelgol Publishing, 2006–, [Online; accessed ¡today¿]. [Online]. Available: http://www.numpy.org/

[46] P. Virtanen, R. Gommers, T. E. Oliphant, M. Haberland, T. Reddy, D. Cournapeau, E. Burovski, P. Peterson, W. Weckesser, J. Bright, S. J. van der Walt, M. Brett, J. Wilson, K. Jarrod Millman, N. Mayorov, A. R. J. Nelson, E. Jones, R. Kern, E. Larson, C. Carey, İ. Polat, Y. Feng, E. W. Moore, J. Vand erPlas, D. Laxalde, J. Perktold, R. Cimrman, I. Henriksen, E. A. Quintero, C. R. Harris, A. M. Archibald, A. H. Ribeiro, F. Pedregosa, P. van Mulbregt, and S. . . Contributors, "SciPy 1.0: Fundamental Algorithms for Scientific Computing in Python," *Nature Methods*, vol. 17, pp. 261–272, 2020.

[47] W. McKinney, "pandas: a foundational python library for data analysis and statistics," *Python for High Performance and Scientific Computing*, vol. 14, 2011.

[48] J. D. Hunter, "Matplotlib: A 2d graphics environment," *Computing in Science & Engineering*, vol. 9, no. 3, pp. 90–95, 2007.